

## Enhanced photocatalytic activity of N, P, co-doped carbon quantum dots: An insight from experimental and computational approach

H.J. Yashwanth<sup>a</sup>, Sachin R. Rondiya<sup>b</sup>, Nelson Y. Dzade<sup>b</sup>, S.D. Dhole<sup>c</sup>, D.M. Phase<sup>d</sup>, K. Hareesh<sup>a,\*</sup>

<sup>a</sup> School of Applied Sciences (Physics), REVA University, Bengaluru, 560064, India

<sup>b</sup> School of Chemistry, Cardiff University, Cardiff, CF10 3AT, Wales, United Kingdom

<sup>c</sup> Department of Physics, Savitribai Phule Pune University, Pune, 411007, India

<sup>d</sup> UGC-DAE Consortium, Indore, 452017, India

### ARTICLE INFO

#### Keywords:

Carbon materials  
Nitrogen  
Phosphorous  
Work function  
Density functional theory

### ABSTRACT

Herein, we demonstrate the single-step microwave radiation assisted approach to develop Nitrogen (N) and Phosphorous (P) co-doped carbon quantum dots (NP-CQD). The developed NP-CQD showed enhancement in visible light photocatalytic activity towards methylene blue dye degradation than that of N-CQD and P-CQD due to creation of energy states and reduced work function as estimated by Ultraviolet photoelectron spectroscopy and corroborated by first-principles Density Functional Theory (DFT) calculations.

The Carbon Quantum Dots (CQD), a new member of carbon family with diameter less than 10 nm, have attracted a lot of attention recently due to their superior properties such as good photostability, high chemical inertness, tunable optical properties and comparatively less toxicity than semiconducting quantum dots [1], leading to their applications in sensors [2], drug delivery [3], bio-imaging [4], photo-catalyst [5], supercapacitors [6], etc. Nevertheless, the remarkable promise of CQD as vital building blocks in nanocomposites and nano devices has not been fully realized [1]. Therefore, the doping of CQD offers a path to create new energy states originated by different electronic configurations of doped atoms thereby enhancing the physico-chemical and catalytic properties [7]. The atomic size of Nitrogen is nearly same as that of Carbon and it has five electrons in its outermost shells, hence Nitrogen is the most effective dopant atom to CQD [4,7]. Furthermore Boron [8], Phosphor [9], Sulfur [7] and Selenium [7] can also be doped to CQD to enhance its optical, sensing, and catalytic properties. Nevertheless, few dopants such as Phosphorus, having its atomic size larger than that of Carbon can also be codoped along with Nitrogen, which can form substitutional energy levels in CQD [4,10–13]. Zhao et al. [4], have developed red emissive CQD by co-doping Nitrogen and Phosphorus using hydrothermal method and applied it for bioimaging and photodynamic therapy of tumor. The Nitrogen and Sulfur codoped CQD were synthesized using a microwave solid-phase pyrolysis method by Liu et al. [10], which showed high enzyme mimics catalytic activity. Yang

et al. [11], have reported the synthesis of Nitrogen and Phosphor doped CQD of size (4–6) nm by hydrothermal method and, it displayed rapid and highly selective detection to nitrite ions in water. The hydrothermal method has been adopted for the synthesis of Nitrogen and Boron codoped CQD with yellow-green emission towards sensing, anti-counterfeiting and cell imaging application by Guo et al., [12]. Recently, Nitrogen and Phosphor codoped CQD of size 5.7 nm have been developed using exothermic reaction for the selective and sensitive detection of trinitrophenol by Babar and Gajre [13]. Nonetheless, there is a lacuna in literature on the validation of experimentally enhanced catalytic properties of co-doped CQD by the theoretically calculated density of states and work function using first principles DFT calculations. Therefore, herein, a single-step microwave radiation assisted method was used for the synthesis of NP-CQD, N-CQD and P-CQD. The synthesized samples were characterized by UV–Visible absorption spectroscopy, X-ray Diffractogram (XRD), High Resolution Transmission Electron Microscopy (HRTEM), X-ray photoelectron spectroscopy (XPS) and Ultraviolet photoelectron spectroscopy (UPS). The visible light photocatalytic activity of synthesized catalysts was studied towards the degradation of methylene blue (MB). Further, the experimentally enhanced photocatalytic activity of NP-CQD was validated through first-principles DFT calculations.

0.1 M of glucose, 6 mM of ethylenediamine and 2 mM of phosphoric acid were mixed in 20 mL of double-distilled water (DDW) and stirred

\* Corresponding author.

E-mail address: [appi.2907@gmail.com](mailto:appi.2907@gmail.com) (K. Hareesh).

<https://doi.org/10.1016/j.vacuum.2020.109589>

Received 22 May 2020; Received in revised form 22 June 2020; Accepted 23 June 2020

Available online 13 July 2020

0042-207X/© 2020 The Authors. Published by Elsevier Ltd. This is an open access article under the CC BY license (<http://creativecommons.org/licenses/by/4.0/>).

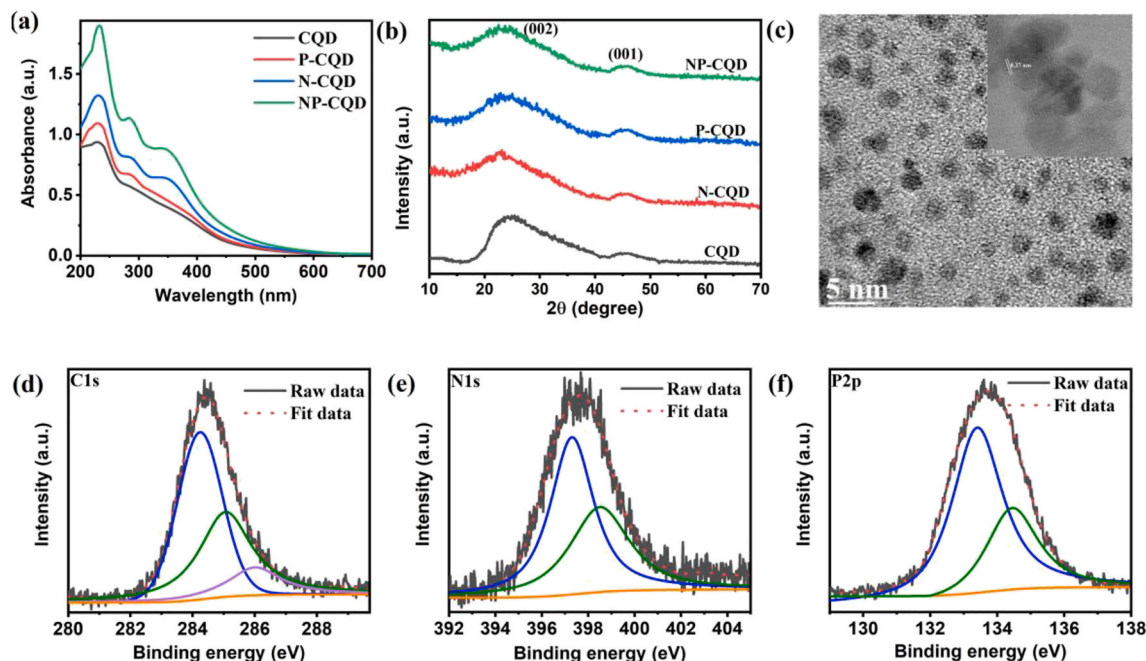


Fig. 1. (a) UV-Visible absorption spectrum; (b) XRD patterns; (c) HRTEM; high resolution XPS of (d) C1s, (e) N1s and (f) P2p of NP-CQD.

for 2 h. Then, it was exposed to household microwave oven of 800 W for 5 min. The unreacted precursors in sample were centrifuged (REMI R-4C) at 12000 RPM for 15 min and supernatant was collected. Further, it was purified using 1 kda dialysis membrane under constant stirring against DDW for 3 days by changing the DDW for every 24 h. The resulting dialyzed solution was freeze-dried to get NP-CQD. Above procedure was used for the synthesis of N-CQD, P-CQD and CQD in the absence of phosphoric acid, ethylenediamine and both respectively. Nevertheless, Li et al. [14], have used microwave assisted method for the synthesis of NP-CQD using ethylenediamine and N-phosphonomethyl aminodiacetic acid at 700 W for 7 min, i.e., the increase in power of microwave decreases the reaction time. JASCO, V-670 spectrophotometer was used to record UV-Visible spectrum. XRD patterns were recorded in Bruker AXS D8 Advance X-ray Diffractometer using X-rays of wavelength  $1.5406 \text{ \AA}$ . HRTEM was carried out using JEOL/JEM 2100 at 200 kV. Omicron EA-125 XPS analyzer was used to record XPS. AIPES beamline (BL-02) at Indus-1 synchrotron source was used to measure UPS. The photocatalytic degradation was carried out using 2 mg of NP-CQD in 20 mL of MB dye (1mg/100 mL) under sunlight with sunshine intensity as  $\sim 832 \text{ W/m}^2$ . The absorbance spectrum was recorded at regular intervals. A similar photocatalytic activity was repeated for N-CQD, P-CQD and CQD. The density functional theory (DFT)

calculations were performed within the VASP package [15] using the dispersion-corrected GGA-PBE functional [16,17]. The kinetic energy cut-off of 600 eV was used to expanded Kohn-Sham (KS) valence states. A graphene hexagonal flake containing 7 hexagons in orthorhombic dimension of  $25 \times 25 \times 25 \text{ \AA}^3$  is used to study the N and P effect on the CQDs. The edge atoms are saturated by hydrogen, i.e.,  $\text{C}_{24}\text{H}_{12}$ . A  $k$ -point mesh of  $1 \times 1 \times 1$  was used to sample the Brillouin zones.

The UV-Visible spectra of N-CQD, P-CQD, NP-CQD is shown in Fig. 1 (a). All the absorption curves exhibited a peak around 233 nm corresponding to  $\pi$ - $\pi^*$  transition of aromatic carbon  $\text{sp}^2$  core domains. Nonetheless, N-CQD, P-CQD, NP-CQD demonstrated a small peak around 285 nm attributed to  $\pi$  system of aromatic ring and, a broad peak around 320–410 nm attributed to  $n$ - $\pi^*$  transition of C=N bearing groups in case of N-CQD and NP-CQD [11,14]. Also, NP-CQD showed a slight red shift of absorption edge signifying the decrease in its bandgap revealing the superior ability to absorb visible light making it a promising catalyst for visible light photocatalytic activity [18]. The XRD pattern (displayed in Fig. 1(b)) of CQD, N-CQD, P-CQD and NP-CQD showed a broad peak around  $24^\circ$  and a weak peak around  $45^\circ$  corresponding to (002) plane ( $d_{002} = 0.38 \text{ nm}$ ) and (100) plane ( $d_{100} = 0.21 \text{ nm}$ ) respectively revealing the amorphous carbon phase as well as partial graphitization in those samples which is in agreement with

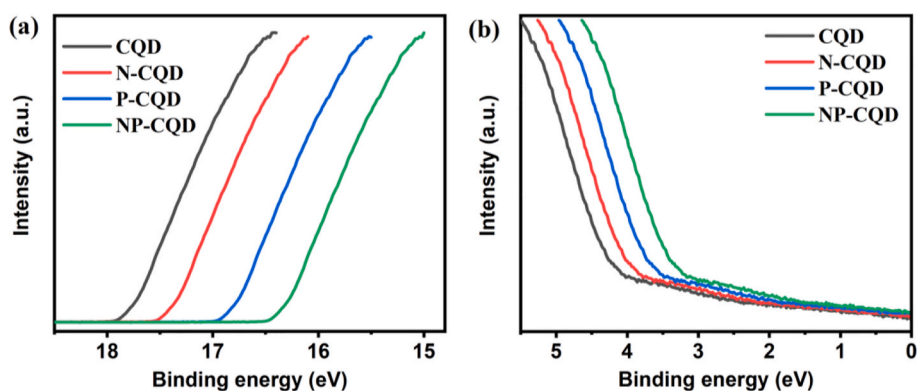
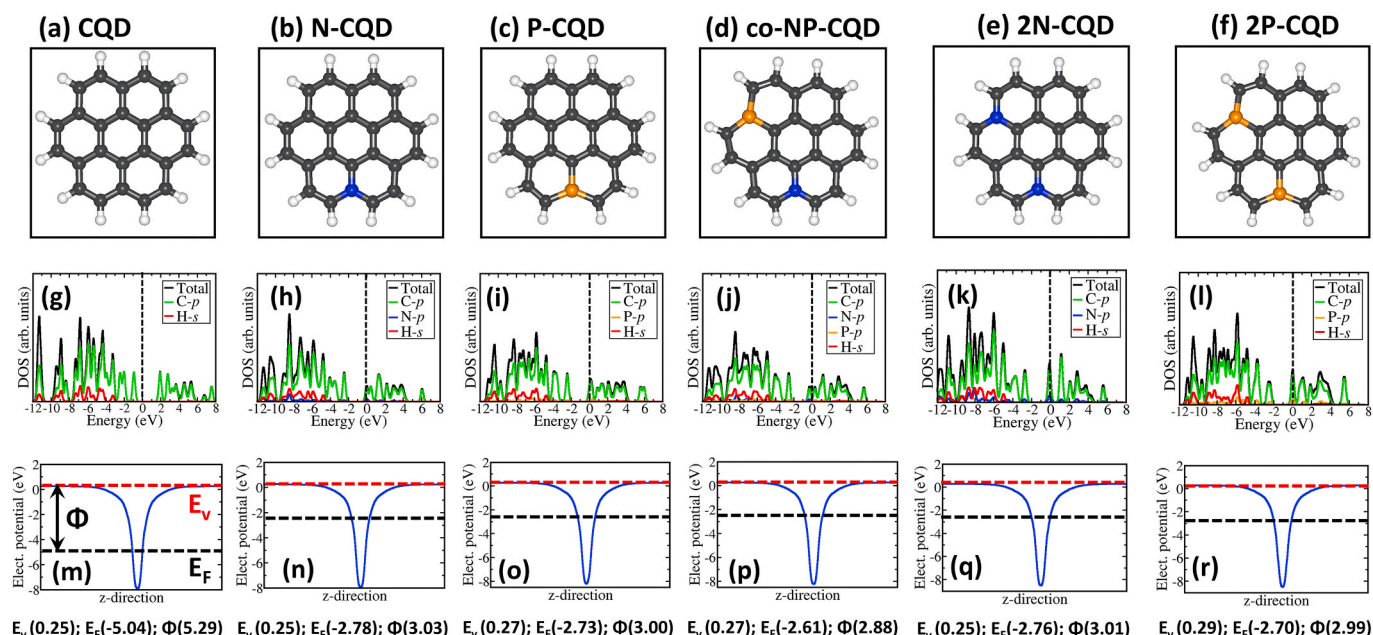


Fig. 2. Ultraviolet photoelectron spectrum of CQD, N-CQD, P-CQD and NP-CQD; (a)  $E_{\text{sec}}$  edge and (b)  $E_{\text{FE}}$  edge.



**Fig. 3.** Optimized structures of pure and doped CQD (a–f), the corresponding PDOS (g–l) and electrostatic potentials (m–r).  $E_v$ ,  $E_F$ , and  $\Phi$  in eV units denotes the vacuum level, Fermi level, and work function. Grey = C; blue = N; orange = P; white = H. (For interpretation of the references to colour in this figure legend, the reader is referred to the Web version of this article.)

already reported results [14,19]. The HRTEM image of NP-CQD (Fig. 1 (c)) reveals monodisperse, spherical shaped quantum dots of size around (2–5) nm without any agglomeration. The distinct interlayer spacing was found to be 0.37 nm (depicting in Inset of Fig. 1(c)) corresponding to (002) plane of NP-CQD corroborating XRD results. The survey scan XPS of CQD, N-CQD, P-CQD and NP-CQD is shown in Fig. S1. NP-CQD of survey scan showed the peaks around 135 eV, 285 eV, 400 eV and 537 eV corresponding to P2p, C1s, N1s and O1s respectively, confirming their presence in NP-CQD. The high resolution XPS of C1s of NP-CQD

depicts in Fig. 1 (d), exhibited 3 peaks at 284.12 eV, 285.24 eV and 286.12 eV due to C=C, carbonyl and carboxyl groups respectively [13]. These oxygen functional groups might have arisen along with P and N doping. Fig. 1(e) depicts high resolution XPS of N1s spectrum which is further deconvoluted into 397.3 eV and 398.5 eV due to C–N–C and N-(C)3 functionalities, respectively [20]. The P2p high resolution XPS as depicted in Fig. 1(f) showed two deconvoluted peaks at 133.41 eV and 134.53 eV, attributed to P2p<sub>3/2</sub> and P–C, respectively [9,13]. The XPS analysis along with UV–Visible spectroscopy, XRD, HRTEM confirmed

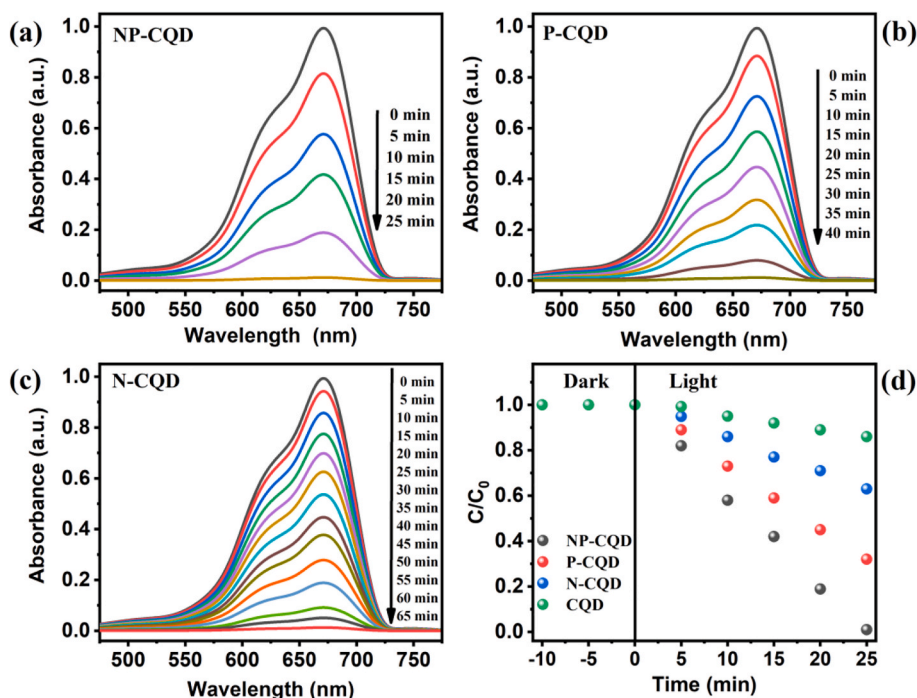


**Fig. 4.** UV–Visible spectrum of MB degradation for (a) NP-CQD; (b) N-CQD; (c) P-CQD and (d) Plot of  $C/C_0$  versus time,  $C$  is concentration of (MB + catalyst) at time ' $t$ ' and  $C_0$  is initial concentration of MB.

the co-doping of Nitrogen and Phosphor in CQD. Recently, Zhang et al., [21] have reported that the inclusion of phosphate material will vary the work function of CQD. Therefore, the work function ( $\phi$ ) of all the sample was calculated from UPS data (displayed in Fig. 2) using equation [18]:  $\phi = hv - |E_{sec} - E_{FE}|$ , where  $hv = 23$  eV, incident photon energy,  $E_{sec}$  is secondary emission onset and  $E_{FE}$  is Fermi edge. The calculated work function was found to be 4.32 eV, 3.07 eV, 3.01 eV and 2.81 eV for CQD, N-CQD, P-CQD and NP-CQD respectively. It is noteworthy to observe that the work function decreased the most for NP-CQD due to N and P co-doping. The extra electrons from N and P will be injected into CQD thereby creating extra energy states, induce a shift of the Fermi energy level closer to the conduction band [22] and thus decrease the work function.

In order to validate the experimentally decreased work function of NP-CQD relative to CQD, DFT was used to calculate work function theoretically. The optimized structures and the corresponding partial density of states (PDOS) and electrostatic potentials of the pure CQD, N-CQD, P-CQD, NP-CQD, 2N-CQD and 2P-CQD are shown in Fig. 3(a–f). It is evident from PDOS (Fig. 3(g–l)) that the doping of CQD with N and P induces a shift in the Fermi level from the valence band edge of the pure CQD to the edge of the conduction, resulting from the introduction of N and P states. The work function of the pure CQD is predicted at 5.29 eV, compared to 3.03, 3.00, 2.88, 3.01, and 2.99 eV for the N-CQD, P-CQD, NP-CQD, 2N-CQD and 2P-CQD, respectively. Fig. 3(m–r) respectively indicating significant reduction in the work function with N and P co-doping. Compared to the 2N and 2P doping (Fig. 3(m–r)), the larger reduction in the work function from the N and P co-doping (Fig. 3p) indicates a synergistic effect between the N and O in the co-doped system. The reduction in the work function of the N and P doped CQD can be attributed to the shifting of Fermi level to higher energy levels (Fig. 3(i–l)) caused by the injection of extra electrons from nitrogen and phosphor to the CQD, as confirmed by the PDOS analyses.

The photocatalytic activity of NP-CQD, N-CQD, P-CQD and CQD was carried out towards the MB dye degradation under sun light and is depicting in Fig. 4(a–d). Fig. 4(a) depicts absorption spectrum of MB exhibiting the main peak around 670 nm due to  $n-\pi^*$  transition and a shoulder band around 620 nm due to  $\pi-\pi^*$  transition (which is not a peak, but a band arises due to vibronic transition) [23,24]. Therefore, a peak around 670 nm is considered for further discussion, which decreased with increase in exposure time for NP-CQD, N-CQD and P-CQD catalyst. Nevertheless, the absorbance diminished completely in case of (NP-CQD + MB) demonstrating the complete degradation of dye. Also, it was found that the NP-CQD exhibited enhancement in MB degradation than that of N-CQD and P-CQD due to decrease in ' $\Phi$ ' as calculated from UPS as well as DFT results. The lower ' $\Phi$ ' of NP-CQD helps to generate photoelectrons much easily compared to the N-CQD and P-CQD. These photogenerated electrons are conveyed to the electron acceptors viz. oxygen molecule thereby effectively creating  $O_2^{\bullet -}$  radicals, which is prevailing oxidizing agent, can degrade dye efficiently in sun light. It is also worth noting that the P-CQD showed more photocatalytic activity than N-CQD, which may be due to its lower work function as predicted from the UPS and DFT results.

The NP-CQD catalyst revealed the enhanced photocatalytic activity towards the degradation of MB dye under sun light compared to N-CQD and P-CQD. The enhanced photocatalytic activity of NP-CQD was

attributed to its reduced work function as predicted from first principles DFT calculations, which points to easier transfer of electrons towards photocatalytic activity processes.

## Declaration of competing interest

The authors declare that they have no known competing financial interests or personal relationships that could have appeared to influence the work reported in this paper.

## Acknowledgements

KH acknowledges financial assistance by DST-SERB, Government of India (No. ECR/2017/002788). SRR and NYD acknowledge the UK-EPSC for funding (Grant No. EP/S001395/1) and Advanced Research Computing at Cardiff (ARCCA) Division, Cardiff University for computer facilities. Information on the data that underpins the results presented here, including how to access them, can be found in the Cardiff University data catalogue at <http://doi.org/10.17035/d.2020.0112140691>.

## Appendix A. Supplementary data

Supplementary data to this article can be found online at <https://doi.org/10.1016/j.vacuum.2020.109589>.

## References

- [1] R. Wang, K.Q. Lu, Z.R. Tang, Y.J. Xu, *J. Mater. Chem.* 5 (2017) 3717–3734.
- [2] V. Singh, *Mater. Lett.* 254 (2019) 415–418.
- [3] M.J. Molaei, *RSC Adv.* 9 (2019) 6460–6481.
- [4] J. Zhao, F. Li, S. Zhang, Y. An, S. Sun, *New J. Chem.* 43 (2019) 6332–6342.
- [5] X. Gao, T.T. Nguyen, X. Gong, X. Chen, Z. Song, W. Du, R. Chai, M. Guo, *Vacuum* 169 (2019) 108912.
- [6] M. Athika, A. Prasath, E. Duraisamy, V.S. Devi, A.S. Sharma, P. Elumalai, *Mater. Lett.* 241 (2019) 156–159.
- [7] S. Wang, J. Sun, X. Li, W. Zhou, Z. Wang, P. He, G. Ding, X. Xie, Z. Kang, M. Jiang, *J. Mater. Chem.* 2 (2014) 8660–8667.
- [8] X. Shan, L. Chai, J. Ma, Z. Qian, J. Chen, H. Feng, *Analyst* 139 (2014) 2322–2325.
- [9] F. Yang, X. He, C. Wang, Y. Cao, Y. Li, L. Yan, M. Liu, M. Lv, Y. Yang, X. Zhao, Y. Li, *Appl. Surf. Sci.* 448 (2018) 589–598.
- [10] T. Liu, Z.W. Cui, J. Zhou, Y. Wang, Z.G. Zou, *Nanoscale Res. Lett.* 12 (2017) 375.
- [11] X. Yang, Y. Zhang, W. Liu, J. Gao, Y. Zheng, *Polyhedron* 171 (2019) 389–395.
- [12] Y. Guo, Y. Chen, F. Cao, L. Wang, Z. Wang, Y. Leng, *RSC Adv.* 7 (2017) 48386–48393.
- [13] D.G. Babar, S.S. Garje, *ACS Omega* 5 (2020) 2710–2717.
- [14] H. Li, F.Q. Shao, S.Y. Zou, Q.J. Yang, H. Huang, J.J. Feng, A.J. Wang, *Microchim. Acta* 183 (2016) 821–826.
- [15] G. Kresse, J. Hafner, *Phys. Rev. B* 50 (1994) 13181–13185.
- [16] J.P. Perdew, K. Burke, M. Ernzerh, *Phys. Rev. Lett.* 78 (1997) 1396.
- [17] S. Grimme, J. Antony, S. Ehrlich, S. Krieg, *J. Chem. Phys.* 132 (2010) 154104.
- [18] K. Hareesh, S.D. Dhole, D.M. Phase, J.F. Williams, *Mater. Res. Bull.* 110 (2019) 82–89.
- [19] P. Wu, W. Li, Q. Wu, Y. Liu, S. Liu, *RSC Adv.* 7 (2017) 44144–44153.
- [20] X.D. Ma, T.T.K. Chi, T.C. Nguyen, V.T. Ta, *Mater. Lett.* 268 (2020) 127595.
- [21] X. Zhang, Q. Zeng, Y. Xiong, et al., *Adv. Funct. Mater.* 30 (2020) 1910530.
- [22] E.C. Silva, F.L. Urias, E.M. Sandoval, B.G. Sumpter, H. Terrones, J.C. Charlier, V. Meunier, M. Terrones, *ACS Nano* 3 (2009) 1913–1921.
- [23] B. Mandal, J. Panda, P.K. Paul, R. Sarkar, B. Tudu, *Vacuum* 173 (2020) 109150.
- [24] P. Chand Sukriti, V. Singh, D. Kumar, *Vacuum* (2020), <https://doi.org/10.1016/j.vacuum.2020.109364>.